Evidence for microbial iron reduction in the methanic sediments of the oligotrophic SE Mediterranean continental shelf

Hanni Vigderovich[1], Lewen Liang[2], Barak Herut[3], Fengping Wang[2], Eyal Wurgaft[1,4], Maxim Rubin-Blum[3] and Orit Sivan[1]

[1]The Department of Geological and Environmental Sciences, Ben-Gurion University of the Negev, Beer-Sheva, 8410501, Israel.
[2] School of Life Sciences and Biotechnology, Shanghai JiaoTong University, Shanghai, 200240, P.R.China.
[3] Israel Oceanographic and Limnological Research, Haifa, 31080, Israel.
[4]Currently: The Department of Marine Chemistry and Biochemistry, Woods-Hole Oceanographic Institution, Woods-Hole, USA
Correspondence to: Orit Sivan (oritsi@bgu.ac.il)

Abstract. Dissimilatory iron reduction is probably one of the oldest types of metabolisms that still participates in important biogeochemical cycles, such as those of carbon and sulfur. It is one of the more energetically favorable anaerobic microbial respiration processes, and is usually coupled to the oxidation of organic matter. Traditionally this process is thought to be limited to the shallow part of the sedimentary column in most aquatic systems. However, iron reduction has also been observed in the methanic zone of many marine and freshwater sediments, well below its expected zone, occasionally accompanied by decreases in methane, suggesting a link between the iron and the methane cycles. Yet, the mechanistic nature of this link (competition, redox or other) has yet to be established, and has not been studied in oligotrophic shallow marine sediments. In this study we present combined geochemical and molecular evidences for microbial iron reduction in the methanic zone of the oligotrophic Southern Eastern (SE) Mediterranean continental shelf. Geochemical pore-water profiles indicate iron reduction in two zones, the traditional one, in the upper part of the sediment, and the deeper zone, located in the enhanced methane concentration layer. Results from a slurry incubation experiment indicate that the deep methanic iron reduction is microbial. The sedimentary profiles of microbial abundance and qPCR of the mcrA gene, together with Spearman correlation between the microbial data and Fe(II) concentrations in the pore-water, suggest types of potential microorganisms that may be involved in the iron reduction via several potential pathways: H_2 or organic matter oxidation, an active sulfur cycle or iron driven anaerobic oxidation of methane. We suggest that intensive upward migration of methane in the sedimentary column and its oxidation by sulfate may fuel deeper microbial activity that allows the observed methanic iron reduction in sediments of the SE Mediterranean.

1 Introduction

Iron (Fe) is the fourth most abundant element in the Earth's crust. It appears as elemental Fe, Fe(II) and Fe(III), and has an important geobiological role in natural systems (Roden, 2006). Dissimilatory microbial ferric iron (Fe(III)) reduction may be one of the first evolutionary metabolisms, and plays a key role in the reductive dissolution of Fe(III) minerals in the natural environment (Weber et al., 2006)

and in the mineralization of organic matter in freshwater sediments (Roden and Wetzel, 2002). It also serves as a redox wheel that drives the biogeochemical cycles of carbon, nitrogen, sulfur and phosphorous (Li et al., 2012 ; Slomp et al., 2013; Sivan et al., 2014; Egger et al., 2016; Ettwig et al., 2016; Riedinger et al., 2017; März et al., 2018).

The dissimilatory iron reduction is part of the anaerobic respiration cascade, in which different organic substrates are used for energy by microorganisms and oxidized to dissolved inorganic carbon (DIC). This is accomplished by reduction of electron acceptors, other than oxygen, according to their availability and energy yield. Denitrification is the first respiratory process in anoxic sediments, followed by manganese reduction, iron reduction and then sulfate reduction. Methane (CH_4) production (methanogenesis) by archaeal methanogens is traditionally considered to be the terminal process of microbial organic matter mineralization in anoxic environments, after the other electron acceptors have been exhausted (Froelich et al., 1979). When the produced methane diffuses away from the methanic layer and meets an electron acceptor it can be consumed by microbial oxidation (methanotrophy). In marine sediments anaerobic oxidation of methane (AOM) coupled to sulfate reduction has been shown to occur (Iversen and Jorgensen, 1985; Hinrichs et al., 1999; Boetius et al., 2000; Orphan et al., 2001; Knittel and Boetius, 2009), and was found to consume up to 90 % of the methane that diffuses upwards to the sulfate methane transition zone (SMTZ) (Niewöhner et al., 1998; Valentine, 2002).

The classical process of dissimilatory iron reduction is coupled to the oxidation of organic matter (organoclastic iron reduction) (Eq. 1, Lovley, 1991; Lovley et al., 1996). However, iron reduction can be coupled to other processes as well, such as hydrogen (H_2) oxidation (hydrogenotrophic iron reduction) (Eq. 1, Lovley, 1991). Besides, iron can be reduced microbially (and also abiotically) by pyrite oxidation (Eq. 2, Bottrell et al., 2000), leading to S intermediates, and followed by their disproportionation to sulfate and sulfide via a "cryptic" sulfur cycle (e.g. Holmkvist et al., 2011).

$$2Fe(III) + organic\ matter/H_2/humic\ acids \rightarrow 2Fe^{2+} + HCO_3^-/CO_2/2H^+ \quad (1)$$

$$FeS_2 + 14Fe^{3+} + 8H_2O \rightarrow 15Fe^{2+} + 2SO_4^{2-} + 16H^+ \quad (2)$$

Another recently discovered pathway of iron reduction is by AOM (Eq. 3).

$$CH_4 + 8Fe(OH)_3 + 15H^+ \rightarrow HCO_3^- + 8Fe^{2+} + 21H_2O \quad (3)$$

This process in marine sediments was evident through incubations of marine seeps (Beal et al., 2009; Sivan et al., 2014). It was also suggested to exist mainly through the modeling of geochemical profiles in deep sea sediments (Sivan et al., 2007; März et al., 2008; Riedinger et al., 2014), and in brackish coastal sediments (Slomp et al., 2013; Segarra et al., 2013; Egger et al., 2015; Egger et al., 2016; Rooze et al., 2016; Egger et al., 2017). In freshwater environments, it was suggested to occur in lakes (Crowe et al. 2011; Sivan et al., 2011; Nordi et al., 2013), and in denitrifying cultures from sewage, where it was performed by methanogens (Ettwig et al., 2016). Iron-coupled AOM in natural lake sediments was indicated using isotope pore-water depth profiles (Sivan et al., 2011), rate modeling based on these profiles (Adler et al., 2011), microbial profiles (Bar-Or et al., 2015), and directly from a set of sediment slurry incubation experiments (Bar-Or et al. 2017). The few microbial studies on iron-coupled AOM

(mainly in cultures) showed the involvement of methanogenic/methanotrophic archaea (Scheller et al., 2016; Ettwig et al., 2016; Rotaru and Thamdrup, 2016; Cai et al., 2018; Yan et al., 2018) or cooperation between methanotrophic archaea and methanogens (Bar-Or et al., 2017).

Whereas Fe(II) is highly soluble, Fe(III) that is the most abundant species of iron natural conditions, appears as low-solubility oxidized minerals. This makes iron usage a challenge to microorganisms, which need to respire these iron-oxide minerals, thus rendering many of the iron-oxide minerals effectively unavailable for reduction and leading to the dominance of sulfate reducing bacteria beyond a certain depth. Therefore, it is not trivial to observe iron reduction below its traditional depth, in the methanic zone, where iron-oxides are assumed to be of low reactivity. Moreover, this type of iron reduction is occasionally accompanied by depletion in methane concentrations, suggesting a possible link between the iron and the methane cycles. There are three potential mechanisms that can link the cycles: 1) a competition between methanogens and iron reducing bacteria over substrates, 2) a metabolism switch of methanogens from methanogenesis to iron reduction, and/or 3) iron coupled AOM, as mentioned above. Previous observations in other environments demonstrated the inhibition of methanogenesis under iron-reducing conditions due to competition between methanogens and iron-reducing bacteria for the common acetate and hydrogen substrates (Lovley and Phillips, 1986; Roden and Wetzel, 1996;Conrad, 1999; Roden, 2003). Different methanogens can also utilize iron directly, by reducing Fe(III). This was shown in pure cultures with the amorphous Fe(III) oxyhydroxide (Bond and Lovley., 2002), in pure cultures close to natural sedimentary conditions (Sivan et al., 2016), in natural lake sediments with different iron oxides (i.e. amorphous iron, goethite, hematite and magnetite) (Bar-or et al., 2017), in anoxic ferruginous lake sediments enrichments (Bray et al., 2018), and in iron-rich clays (Liu et al., 2011; Zhang et al., 2012; Zhang et al., 2013).

Despite the above studies, the nature of the link between the iron and the methane cycles in marine's methanic zone, which creates suitable conditions for iron reduction, has not yet been determined. Furthermore, this microbial iron reduction in the methanic zones has not been shown in the sediments of oligotrophic shallow marine environments. In this study we report observations of microbial iron reduction in the methanic depth of marine sediments from the oligotrophic SE Mediterranean continental shelf. This is by using both geochemical pore-water profiles and microbial profiles at three different stations combined with a simple slurry incubation experiment from the methanic zone. The slurries were amended with hematite and magnetite, as, given their low reactivity, these are the expected Fe(III) minerals to survive the sulfide zone (Canfield, 1989; Poulton et al., 2004). Furthermore, these minerals were found to be active in iron-coupled AOM in lake sediments (Bar-Or et al., 2017). The profiles and the incubation experiment, including the related microorganisms, are discussed in terms of the possible links between the cycles of iron and methane.

2 Methods

2.1 Study site

The Levantine Basin of the SE Mediterranean Sea, including Israel's continental shelf, is an oligotrophic nutrient-poor marine system (Herut et al., 2000; Kress and Herut, 2001). The continental shelf narrows

from south to north and compromises of Pliocene-Quaternary Nile-derived sediments. The sedimentation rate decreases with increasing distance from the Nile Delta and from the shoreline (Nir, 1984; Sandler and Herut, 2000). Off the shore of Israel the sedimentation rate is a relatively high at ~0.1 cm y^{-1} (Bareket et al., 2016). The bottom seawater along the continental shelf is well oxygenated and sulfate concentrations at the water-sediment interface are ~30 mmol L^{-1} (Sela-Adler et al., 2015). While the highest levels of total organic carbon (TOC) (1 – 2%) in sediments were found in the Western Mediterranean Basin and offshore the Nile River delta, the central and eastern regions of the Levantine Basin have relatively low TOC levels (~0.1 – 1.4%; Almogi-Labin et al., 2009; Sela-Adler et al., 2015; Astrahan et al., 2017). Along the Egyptian coast, the TOC in surface sediments on the shelf reaches maximum values of 1.5% (Aly Salem et al., 2013). The finding of a 'gas front' in seismic profiles within the sediments of the continental shelf of Israel (Schattner et al., 2012), led to the discovery of biogenic methane formation at some locations in shallow sediments (Sela-Adler et al., 2015).

2.2 Sampling

Seven sediment cores (~5 – 6 m long) were collected using a Benthos 2175 piston corer, from the undisturbed seafloor sediments of the SE Mediterranean continental shelf of Israel at water depths of 81 – 89 m from three stations; SG-1, PC-3 and PC-5 (Fig 1). The cores were sampled during cruises of R.V. *Shikmona* between 2013 to 2017, and by the R.V. *Bat-Galim* on January 2017 (Table 1). The sediment cores were sliced on board every 25 – 35 cm within minutes upon retrieval from the seafloor. This area was previously investigated for other purposes, such as the sulfate reduction in the SMTZ (Antler et al., 2015; Wurgaft et al., 2019.), and methanogenesis characteristics (Sela-Adler et al., 2015).

From each interval, a 2.5 mL of total sediment sample was collected and inserted immediately into an anaerobic 10 mL glass bottle filled with 5 mL NaOH 1.5 N for headspace measurements of methane concentration (after Nusslein et al, 2003). In addition, another 2.5 mL sediment sample was taken from each segment of the cores and transferred into a 20 mL glass bottle filled with NaCl saturated solution for H_2 concentrations measurements. Sediment samples from each segment of the cores were centrifuged on board if possible or in the lab within a day by Sorval centrifuge at 9500 RPM under 4 °C and Ar atmosphere in order to extract pore-water for chemical analysis. The supernatant was filtered (0.22 µm) and analyzed for Fe(II), sulfate, sulfide, DIC and the stable carbon isotope composition of the DIC ($\delta^{13}C_{DIC}$). After the pore-water extraction, the sediment was analyzed for the content of the different reactive iron minerals (Table 2). In addition, sediment sub-sample from each segment of the January 2017 core from SG-1 station was kept at -20 °C for molecular analysis. Due to high water content and movement in the uppermost part of the sediments, two ~30 cm sediment cores were also sub-sampled separately, using a 0.0625 m^2 box corer (Ocean Instruments BX 700 Al) and Perspex tubes during the September 2015 and January 2017 cruises. The short cores were stored at 4 °C, cut in the lab within 24 hours after their collection and their results are presented for the top sediment (Fig. 2).

2.3 Slurry incubation experiment

The experimental set-up consisted of 11 bottles with sediment from the methanic zone (265-285 cm depth) from Station SG-1, where iron reduction was apparent in the pore-water profiles (Fig 2). Prior to

the beginning of the experiment, sediment from the designated depth had been homogenized in an anaerobic bag under N_2 atmosphere. It was then transferred under anoxic conditions to a 250 mL glass bottle with the addition of synthetic sea water without sulfate to reach 1:1 sediment – water slurry ratio for 3 months incubation period. After the incubation period the slurry was sub-divided anoxically to the 11 experiment bottles (60 mL each), and synthetic sea water was added for final sediment – water ratio of 1:3. The bottles were sealed with a crimped cap and were flushed with N_2 for 5 minutes, shaken vigorously and flushed again, (repeated 3 times). Three experimental bottles were autoclaved twice to serve as "killed" control for the experiment. The experimental bottles were amended with 1.6 g L^{-1} of hematite (Fe_2O_3) or 2.3 g L^{-1} of magnetite (Fe_3O_4) to reach Fe(III) final concentration of 10 mmol L^{-1}. The three killed bottles were amended with the iron oxides after they cooled down to room temperature. H_2 was added to some treatments to test its potential as an electron donor. One mL of H_2 was injected by gas tight syringe to the three killed bottles, to two bottles with the addition of hematite and to two bottles with the addition of magnetite (to reach final concentration of ~4% of the head space volume). The experimental bottles were sampled several times for dissolved Fe(II) concentrations during the 14 day experiment period.

2.4 Analytical methods

2.4.1 Pore-water analyses

Methane concentrations were analyzed by Focus Gas Chromatograph (GC; Thermo) equipped with FID detector with detection limit of 50 µmol L^{-1}. H_2 concentrations were analyzed in a Reducing Compound Photometer Gas Chromatograph (RCP-GC; Peak Laboratories). Dissolved Fe(II) concentrations were measured using the ferrozine method (Stookey, 1970) by a spectrophotometer at 562 nm wavelength with detection limit of 1 µmol L^{-1}. Sulfide was measured using the Cline (1969) method by a spectrophotometer at 665 nm wavelength with detection limit of 1 µmol L^{-1}. Total sulfur concentrations were measured in an inductively coupled plasma atomic emission spectrometer (ICP-AES), Perkin Elmer Optima 3300, with an analytical error of ±1% (average deviations from repeated measurements of a seawater standard). Since sulfide was not detected in any of the sediment cores, the measured total sulfur concentrations were assumed to be sulfate concentration. The $\delta^{13}C_{DIC}$ values were measured on a DeltaV Advantage Thermo© isotope-ratio mass-spectrometer (IRMS) at a precision of ±0.1 ‰. Results are reported versus VPDB standard. Several pore-water profiles of dissolved total sulfur, CH_4, $\delta^{13}C_{DIC}$, Fe(II) and H_2 were produced during the study, and all of them are presented. For each profile, the error bar is that of the average deviation of the mean of the duplicates, in cases where they were taken, otherwise it is that of the analytical error (if larger than the symbol).

2.4.2 Sediment analysis

Reactive Fe(III) in the sediments was measured according to Poulton and Canfield (2005) definition and sequential extraction procedure. The different reactive iron minerals were separated to (1) carbonate-associated Fe; (2) easily reducible oxides; (3) reducible oxides and (4) magnetite. About 0.6 g dry sediment was inserted to a centrifuge tube with 10 ml of a specific extractant at every stage under oxic conditions and constant agitation (Table 2). The fluids were separated from the sediment by centrifugation and removed from the tube with Pasteur pipette after every extraction stage. At the end of each extraction stage, the extractant was transferred to a 15 mL falcon tube with 0.1 mL ascorbic acid and 0.1 mL ferrozine solution to reduce all the Fe(III) to Fe(II) and fix it, then it was measured spectrophotometrically. The results presented as "total reactive Fe(III)" are the sum of the easily reducible oxides, reducible oxides and magnetite. Pyrite profile was produced by Wurgaft et al., (2019).

2.4.3 Quantitative PCR and 16S rRNA gene V4 amplicon pyrosequencing

DNA was extracted from the sediment core of Station SG-1 from January 2017 using Power Soil DNA Kit (MoBio Laboratories, Inc., Carlsbad, CA, USA) following manufacturer's instructions. Copy numbers of selected genes were estimated with quantitative PCR (qPCR) as described previously (Niu et al., 2017) using specific primers: Uni519f/Arc908R and bac341f/519r for archaeal and bacterial 16S rRNA genes, respectively, and mlas/mcrA-rev for the *mcrA* gene, which encodes the α-subunit of methyl-coenzyme M reductase. The amplification efficiency was 94.5%, 106.3% and 92.4% for the archaeal 16S rRNA, bacterial 16S rRNA and the *mcrA* gene, respectively (the respective R^2 of the standard curve was 0.998, 0.998 and 0.995).

The V4 regions of bacterial and archaeal 16S rRNA genes were amplified using barcoded 515FB/806RB primers (Walters et al., 2015) and Arch519/Arch806 primers (Song et al., 2013), respectively. PCR mixture contained 6 – 10 ng total DNA, 5 μL 10× Ex Taq buffer, 4 μL 2.5 mmol L^{-1} dNTP mix, 1 μL of each primer, 0.25 μL Ex Taq polymerase (Ex-Taq; TaKaRa, Dalian, China) and 5 μL bovine serum albumin (25 mg mL^{-1}) in a total volume of 50 μL. DNA was sequenced as 2x150 bp reads using Illumina MiSeq platform (Illumina, USA). Sequence quality assessments, chimera detection and down-stream phylogenetic analyses were conducted in QIIME (Caporaso et al., 2010). Taxonomical assignments for each OTU were performed in QIIME using the BLAST method and the SILVA128 reference database. 24056 to 132042 high quality sequences were obtained per sample, with the proportion of high-quality sequence versus total sequence between 81.97 – 99.89%. Spearman correlation was performed using the online calculator (http://www.sthda.com/english/rsthda/correlation.php) to test the relevance of microbial abundance and communities with Fe(II) concentration along the depth of the sediment core from 185 cm to the bottom 575 cm, which is the methanic zone of the sediment core according to the geochemical profile (see the results below).

3 Results

3.1 Geochemical profiles

Geochemical pore-water profiles of several sediment cores from the three stations (SG-1, PC-3 and PC-5 (Fig. 1, Table 1)) were produced in order to investigate the iron reduction process in the methanic zone of the SE Mediterranean continental shelf and its potential sources. The pore-water profiles from Station SG-1 (Fig. 2) show complete depletion of total sulfur at approximately 150 cm depth in all the station cores. Sulfide concentrations were below the detection limit in all cores, indicating that the total sulfur is mostly sulfate. Methane concentrations show an increase with depth immediately after the consumption of sulfate. The maximum methane concentration was approximately 10 mmol L^{-1} at ~140 cm depth in June 2015. The other methane depth profiles show an increase in the concentrations to approximately 2 mmol L^{-1} and then leveling off throughout the bottom of the cores (~600 cm). Detected dissolved Fe(II) concentrations were found in the traditional iron reduction zone in the upper part of the sediment (between 30 – 90 cm depth), and a second peak was found in the deeper part of the sediment, at the methanic zone (below 180 cm depth). Maximum dissolved Fe(II) concentrations reached 84 µmol L^{-1} in the traditional iron reduction zone of the sediment cores and 65 µmol L^{-1} in the methanic zone. The $\delta^{13}C_{DIC}$ values were the lowest (-35 ‰), as expected, at the SMTZ depth, and the highest in the methanic zone. H_2 concentrations decreased to a minimum of 0.017 µmol L^{-1} at 155 cm depth, and then increased to a maximum of 0.147 µmol L^{-1} at 485 cm depth.

Pore-water profiles from Station PC-3 (Fig. 2) show similar patterns to Station SG-1 on all three sampling dates, but with lower methane concentrations and deeper SMTZ. Total sulfur was completely depleted within the upper 300 cm depth. Sulfide concentrations were below the detection limit at this station as well. Methane profiles show an increase in methane concentration immediately after the consumption of sulfate. The maximum methane concentration reached 0.8 mmol L^{-1} at 450 cm depth in the Aug-13 core. The Fe(II) profiles show two peaks also here, one in the upper part of the sediment with maximum value of 32 µmol L^{-1} at 177 cm depth, and another one with maximum value of 64 µmol L^{-1} at 390 cm depth at the methanic depth. The $\delta^{13}C_{DIC}$ values decreased from approximately -10 ‰ at the water-sediment interface to -20 ‰ at the SMTZ. Below that zone there was an increase in $\delta^{13}C_{DIC}$ values to about -5 ‰ due to methanogenesis. H_2 concentrations remained around 2 µmol L^{-1} along the core. The three deviating points that do not fit the clear pattern are attributed to an analytical or sampling error.

Pore-water profiles from the core collected at Station PC-5 (Fig. S1) resembles the profiles of Station PC-3. Total sulfur was depleted at approximately 300 cm, and methane concentrations increased below that depth to 0.3 mmol L^{-1}. The Fe(II) profile shows two peaks in this core as well, one in the upper sediment of 20 µM at 150 cm depth and the second of 30 µmol L^{-1} in the methanic zone. The $\delta^{13}C_{DIC}$ value decreased from -5 ‰ at the water-sediment interface to -25 ‰ at the SMTZ, and below that depth increased to -17 ‰ at the methanic zone.

In addition to the dissolved constituents' profiles, reactive iron minerals were extracted from the sediment collected on September 2015, and iron minerals profiles from Stations SG-1 and PC-3 were produced (Fig. 2). In Station SG-1 there appears to be a slight variability in the content of the minerals. The Fe-

carbonate minerals (i.e. siderite and ankerite) content in the upper part of the sediment was 0.22 dry wt%, increased to ~0.45 dry wt % at 103 cm depth and then remained constant. The iron (hydr)oxides (i.e. ferrihydrite and lepidocrocite) content was 0.49 dry wt % in the upper part of the sediment, peaked at 203 cm depth to 0.64 dry wt % and then decreased to 0.50 dry wt % at the bottom of the core. The reducible oxides (i.e. hematite, goethite and akageneite) content was 2.15 dry wt % in the upper part of the sediment, decreased to 1.03 dry wt % at 312 cm depth, and then it increased to 1.55 dry wt % at 427 cm depth. Magnetite content was 0.34 dry wt % in the upper part of the sediment, decreased to 0.32 dry wt % at 153 cm depth, increased to 0.35 at 253 cm depth, decreased to 0.23 dry wt % at 312 cm depth, and increased again to 0.35 dry wt % at the bottom. A pyrite content profile from Station SG-1 was also produced from the September 2015 cruise data and shows two peaks; the first of 1.10 wt % at 153 cm depth, and the second of 1.80 wt % at 312 cm depth. The total reactive Fe(III) oxides profile showed a general decrease from 3.00 dry wt % at 13 cm depth to 2.27 dry wt % at 507 cm depth, with two minimum peaks of 2.42 dry wt % at 103 cm and of 1.88 dry wt % at 312 cm.

In Station PC-3 there appeared to be smaller changes in the different reactive oxides with depth (Fig. 2). The Fe-carbonate minerals content in the upper part of the sediment was 0.50 dry wt % and reached 0.69 dry wt % in the deep sediment. The iron (hydr)oxides concentrations were approximately 1.00 dry wt % throughout the sediment column. The reducible oxides concentrations were 0.78 dry wt % in the upper part of the sediment, increased to 0.89 dry wt % at 167 cm depth and then decreased to 0.76 dry wt % at 495 cm depth. Magnetite concentration was 0.83 dry wt % in the upper part of the sediment, increased to 0.89 dry wt % at 167 cm, and then decreased again to 0.75 dry wt % at 495 cm depth. The total reactive Fe(III) oxides content varied between 2.10 dry wt % (at 167 cm depth) and 1.76 dry wt % (at 137 cm depth).

3.2 Abundance and diversity of bacteria and archaea

The qPCR of bacterial and archaeal 16S rRNA genes from the SG-1 core (collected on January 2017) revealed an abundance of bacterial genes between $1.46 – 9.45\times10^6$ copies per g wet sediment, while that of archaea was between $8.15\times10^5 – 2.25\times10^7$ copies per g wet sediment (Fig. 3). The abundance of bacteria and archaea decreased gradually in the top 95 cm, increased sharply at 125 cm depth within the SMTZ, remained relatively stable with high abundance at 185 – 245 cm (the top layer of the methanic zone), and then decreased. Notably, the abundance of both bacteria and archaea peaked within the methanic zone at 245 cm in correspondence with a Fe(II) concentration peak. However, it is not feasible to compare the abundance of archaea and bacteria by this method due to bias caused by the PCR primers used (Buongiorno et al., 2017). The abundance of the *mcrA* gene increased sharply from the surface layer to the SMTZ, peaked at 155 cm and remained stable at 155 – 245 cm, indicative of active anaerobic methane metabolism in the SMTZ and an active methanic zone (Fig. 2). Spearman correlation test (Table S2) shows that the abundance of the bacteria and archaea 16S rRNA genes and *mcrA* genes correlated with Fe(II) concentration in the methanic zone, where *mcrA* gene correlated the most significantly ($r = 0.5429$, p value = 0.04789).

Illumina-sequencing of the 16S rRNA gene revealed diverse bacterial and archaeal communities throughout the SG-1 core (Fig. 4). Although no clear plateau was observed on species rarefaction curve for the current sequencing depth (Fig. S2), Shannon diversity indices reached stable values, indicating that those sequences well covered the diversity of bacterial and archaeal populations in the samples (Fig. S3). Shannon index, based on 16S rRNA gene sequences, shows higher diversity in the top layers of the sediment along with similar values through the core using the bacterial primers, while for sequences using archaeal primers, the values varied in different layers (Table S1). The bacterial sequences were affiliated with the following phyla: Planctomycetes (25.7%), Chloroflexi (23.2 %), Proteobacteria (12.9%), Deinococcus-Thermus (9.9 %), Acidobacteria (3.5%), Aminicenantes (3.3 %), Spirochaetes (2.3%), Deferribacteres (1.7%), Elusimicrobia (1.6%), Aerophobetes (1.6%), Nitrospirae (1.4%), Firmicutes (1.4 %), Actinobacteria (1.4 %), TM6 (Dependentiae) (1.2%), Marinimicrobia (SAR406 clade) (1.0%), and other taxa with less than 1% of the bacterial communities (Fig. 4a). Bathyarchaeota were the predominant archaea in all the sediment layers, based on the high relative abundance of their 16S rRNA gene sequences (91.0%). The remaining archaeal phyla comprised Euryarchaeota (3.2%), Thaumarchaeota (2.4%), Lokiarchaeota (1.0%), and other phyla with less than 1% of the archaeal communities (Fig. 4b). Spearman correlation analysis (Table S2) revealed that uncultured SBR1093 ($r = 0.6176$, p value = 0.01859) from bacterial Candidate Phylum SBR1093, subgroup 26 of Acidobacteria ($r = 0.5841$, p value = 0.02828), the uncultured bacterium from TK10 Class of Chloroflexi phylum ($r = 0.5297$, p value = 0.0544) and *uncultured Bathyarchaeota sp*. (archaea) ($r = 0.5516$, p value = 0.04388) correlated significantly with Fe(II) concentration.

3.3 Incubation experiment

Sediment from the observed deep iron reduction zone of Station SG-1 from January 2017 core was used for a simple short-term (couple of weeks) slurry incubation experiment in order to characterize the iron reduction process in the methanic zone. Hematite and magnetite, which were expected to survive the sulfate zone, and were shown to be a source for AOM in lake sediments, were added to the slurries. Indeed, the iron oxide profiles (Fig. 2) confirm that hematite and magnetite were abundant in the methanic zone in this core. Hydrogen was added as well to some of the bottles.

The results of the experiment are shown in figure 5. Dissolved Fe(II) concentrations show significant increase from 11 $\mu mol\ L^{-1}$ to approximately 90 $\mu mol\ L^{-1}$ during the first three days in all the experimental bottles, except for the killed bottles, implying that the reduction is microbially mediated. Another observation was that the microorganisms were able to reduce both hematite and magnetite to the same extent. In addition, no difference in the Fe(II) concentrations between bottles with and without the addition of H_2 was observed.

4 Discussion

4.1 General

This study was performed in the SE Mediterranean (Fig. 1) in the area of the recently discovered 'gas front' (Schattner et al., 2012), where biogenic methane was found at some locations in shallow sediments with low TOC content (Sela-Adler et al., 2015). Station SG-1 is located at the center of this area, while

PC-3 and PC-5 stations at the edges, and indeed methane related processes were more intensive at station SG-1, linking the shallow sediment processes to this reservoir. Our results suggest that there are two sources for methane in the sediment: the first is from migration of methane from this gas front area (Wurgaft et al., 2019), and the second is from *in-situ* formation. *In-situ* methanogenesis in the shallow shelf sediments is evident by the geochemical profiles of $\delta^{13}C_{DIC}$ and $\delta^{13}C_{CH4}$ (Sela-Adler et al., 2015) and by the microbial profiles of population and functional *mcrA* gene (Figs. 3 and 4, further discussed below).

The comparison between the sites shows that methane reaches the highest concentrations, up to its saturation level, at Station SG-1 (Sela-Adler et al., 2015), specifically in the profile from June 2015. This leads to intensive AOM by sulfate at the SMTZ, causing it to occur at shallower depth and to produce lower $\delta^{13}C_{DIC}$ values than the other two stations. The relation between the upward fluxes of methane, the SMTZ depth and the $\delta^{13}C_{DIC}$ values fits previous studies (e.g. Sivan et al., 2007). The higher methane concentrations in the June 2015 profile is presumably due to intensive migration of methane from the deeper sediments and/or more intensive methane production at the exact location of the core collected at that time. The H_2 concentrations at Station SG-1 were lower by two orders of magnitude than the concentrations at Station PC-3. This is possibly due to the more intensive hydrogen consuming processes at SG-1. Fe(II) profiles show some variability between the cores within the same station. This is reasonable as iron reduction is sensitive to environmental changes such as shifts in local pH, the different types of electron shuttles, and organic compounds that are present in the surroundings.

Despite the pore-water profiles variability between the stations, they show a resemblance in their trends. All geochemical pore-water and reactive Fe(III) profiles suggest that the sediments in this area of the SE Mediterranean shelf can be classified into three general depth-zones (Fig. 2): **zone 1** is the upper part of the sediment, where the traditional classical iron reduction occurs, probably coupled to organic matter oxidation, with sulfate reduction below it; **zone 2** is the SMT depth, where methane starts to increase, sulfate is completely depleted, and Fe(II) is either present in low concentrations or absent (probably due to the precipitation of iron-sulfide minerals). In addition, the $\delta^{13}C_{DIC}$ values are the lowest in this zone, as expected from the intensive AOM process there, which uses the isotopically light carbon of the methane as a carbon source with a small fractionation (Whiticar, 1999); **zone 3** is the methanic zone, where methane concentrations increased to the highest values in all stations, as did the $\delta^{13}C_{DIC}$ since the carbon source for the methane comes mainly from CO_2, leaving the residual DIC heavier by about 60 ‰ (Whiticar, 1999). At this zone, local maxima of Fe(II) concentrations in the pore-water were found in all cores, indicating reduction of iron oxides. The slurry experiment results show only a slight increase in Fe(II) concentrations in the killed bottles compared to their significant increase in the non-killed bottles, inferring that the iron reduction in zone 3 is microbial (Fig. 5).

4.2 Potential methanic iron reduction pathways

The observed intensive iron reduction in the methanic sediments is the first in the SE Mediterranean shelf. The phenomenon of iron reduction in the methanic depth has been observed before in other marine provinces (Jorgensen et al., 2004; März et al., 2008; Slomp et al., 2013; Riedinger et al., 2014; Treude et al., 2014; Egger et al., 2016). Yet, the type of link to the methane cycle is not well understood. Usually,

iron reduction is coupled to oxidation of organic matter (Lovley and Phillips, 1988) and is performed by iron reducing bacteria, which is probably the case in zone 1. It is however questionable if this also stands for zone 3 and if not, what process is responsible for the iron reduction at this depth and its relation to methane. The iron reduction in zone 3 can occur potentially via four pathways: 1) oxidation of organic matter arriving from the SMTZ, where it is produced by the upward migrating methane, 2) oxidation of the methane itself, 3) H_2 oxidation or 4) oxidation of sulfur species through a cryptic cycle.

The oligotrophic nature of the studied area would suggest that intensive bacterial iron reduction coupled simply to the oxidation of organic matter in zone 3 is less likely. The low nutrient and low chlorophyll concentrations in the water column results in low TOC amounts in the sediments (Sela-Adler et al., 2015). Nevertheless, we observe high methane concentrations in zone 3 in all three stations, where part of it is from upward migration. This indicates that regardless of the area's present oligotrophic nature, the TOC substrate may be enough to sustain all the microbial activity and to take part in the iron reduction process in the methanic zone, just from biomass production in the SMTZ and its fast use below (so the TOC content seems still low).

The importance of the methane flux as a carbon source that supports the deep microbial community in the sediments of the SE Mediterranean can be illustrated by comparing the organic carbon flux from the photic zone, with the flux of organic carbon that is oxidized by sulfate in the pore-water. Using traps, Moutin and Raimbault (2002) estimated an export flux of 7.4±6.3 mgC m^{-2} d^{-1}, which leaves the photic zone. However, Wurgaft et al. (2019) estimated that the flux of DIC toward the SMTZ from sulfate reduction is equivalent to 8±3 mgC m^{-2} d^{-1}. Whereas the difference between the two fluxes is statistically insignificant, it should be noted that the flux of organic material that survives aerobic oxidation in the water column and the upper part of the sediment column, as well as anaerobic oxidation by other electron acceptors with higher energy yield (Froelich et al., 1979; Emerson et al., 1980), is likely to be substantially smaller than the flux measured by Moutin and Raimbault (2002). Therefore, it is unlikely that export flux from the photic zone constitutes the sole source of carbon to the SMTZ. Wurgaft et al. (2019) suggested that "external" methane, originates in deeper portions of the sediments, provides important source of carbon to the SMTZ in Station SG-1. Such fluxes of "external" methane are common along continental margins sediments (e.g. Milkov and Sassen, 2002; Milkov, 2004; Zhang and Lanoil, 2004; Paull et al., 2008). Here, we suggest that this supply of methane, leads to intensive sulfate-mediated AOM in the SMTZ, and that this intensive process and biomass may serve as an additional substrate that "fuels" the deeper zone, activating the iron-oxides.

The recently discovered iron-coupled AOM process (Eq. 3) is the second potential process that can involve iron-oxide reduction in the deep methanic zone (Sivan et al., 2011: Segarra et al., 2013; Slomp et al., 2013; Riedinger et al., 2014; Egger et al., 2015; Rooze et al., 2016; Bar-Or et al., 2017; Egger et al., 2017). Fe(III) as an electron acceptor for AOM provides a greater free energy yield than sulfate (Zehnder and Brock, 1980), and its global importance was emphasized (Sivan et al., 2011: Segarra et al., 2013; Sivan et al., 2014). Two of the main environmental conditions for iron-coupled AOM to occur are high dissolved methane concentrations and abundant reducible iron oxides (Egger et al., 2017). Thus, from our profiles it seems that AOM could be a valid option, considering the high methane concentrations

411 and the high sedimentation rates (0.1 cm y^{-1} (Bareket et al., 2016)), which allow the iron oxides to survive
412 the sulfidic zone and reach the methanic zone (Egger et al., 2017). This can also be inferred from figure
413 6, where some association was observed between the dissolved Fe(II) concentrations and the methane
414 concentrations in zone 3. It seems that at high concentrations of Fe(II) methane concentrations are low
415 and vice versa. This could be a result of iron-coupled AOM that uses methane to reduce Fe(III)-oxides,
416 releasing dissolved Fe(II) to the pore-water. It can also suggest a type of competitive relationship between
417 methanogenesis and microbial iron reduction, or microbial population switching from methanogenesis
418 to iron reduction metabolism (e.g. Sivan et al., 2016). It should be noted that our experiment was not
419 designed to test AOM due to its short time scale of a few weeks, hence another long experiment with the
420 addition of the ^{13}C-labeled methane will enable us to shed more light on this association.

421 The third potential process that can be coupled to iron reduction in the methanic zone is H_2 oxidation
422 (Eq.1). H_2 is an important intermediate in anoxic aquatic sediments. In this type of environment, it is
423 produced mainly by fermentation of organic matter (Chen et al., 2006), and can be involved in different
424 microbial processes where each process would need a certain amount of H_2 in order to occur (Lovley and
425 Goodwin, 1988). The H_2 levels at SG-1 and PC-3 stations (Fig. 2) are relatively high in comparison to
426 other marine environments (Lilley et al., 1982; Novelli et al., 1987), suggesting that there is enough H_2
427 to sustain the iron reduction process. The increase in H_2 concentration profile at the methanic zone in
428 SG-1 station could be explained by the occurrence of fermentation processes, which enables H_2 to
429 accumulate (Chen et al., 2006). The H_2 involvement was tested by injecting 1 mL of this gas to the
430 experimental bottles in the methanic iron reduction process (Fig. 5). We observed that the increase of
431 Fe(II) concentration was similar in the bottles with H_2 addition compared to the bottles without H_2. This
432 could mean that either there is enough H_2 in the sediments as it is, as implied by the H_2 pore-water
433 profiles, or that at the methanic depth H_2 is not involved in the iron reduction process.

434 The fourth potential way to reduce iron in zone 3 is by an active sulfur cycle. The pyrite profile supports
435 this possibility by showing two peaks, one in zone 2 of ~1 wt% and the second in zone 3 of ~2 wt% at
436 about 300 cm depth (Fig. 2). The peak at 300 cm depth indicates possible active sulfur cycle, even though
437 sulfate is already undetected at 200 cm. Thus, a possible scenario is that Fe(III) is reduced by pyrite
438 oxidation (Eq. 2) (Bottrell et al., 2000), which triggers the 'cryptic' sulfur cycle, as observed in other
439 marine sediments (Holmkvist et al., 2011; Brunner et al., 2016; Egger et al., 2016). In this cycle,
440 elemental sulfur, and eventually by disproportionation also sulfide and sulfate, are produced. The sulfide
441 reacts with iron-oxide and precipitates as FeS or as pyrite (Holmkvist et al., 2011). The sulfate can inhibit
442 methanogenesis (Mountfort et al., 1980; Mountfort and Asher, 1981), which can result in the
443 enhancement of the iron reduction process due to competition for substrate with the methanogenesis
444 process. Another indication for an active sulfur cryptic cycle comes from the 16S analysis (Fig. 4), which
445 shows that Proteobacteria, a potential sulfur related bacteria phylum, is one of the most abundant phyla
446 in the sediments. Moreover, the increase in the abundance of Sva0485 order of the deltaproteobacteria
447 class, a known sulfate reducer (Tan et al., 2019) with depth, supports an active sulfur cycle in zone 3 as
448 well.

449 **4.3 Potential microbial players**

450 Our data profiles and incubations indicate that the observed iron reduction in the methanic zone of the
451 SE Mediterranean shelf is performed by microbial activity. The microbial results show first that the
452 abundances of the bacteria and archaea (Fig. 4) are typical to oligotrophic marine sediments (e.g. South
453 China Sea that contains ~0.5 – 1 % TOC (Yu et al., 2018)). Second, even though potential bacterial iron
454 reducers, such as *Alicyclobacillus*, *Sulfobacillusin*, *Desulfotomaculum* genera (Firmicutes), *Acidiphilium*
455 (Alphaproteobacteria), *Desulfobulbus*, *Desulfuromonas*, *Geobacter*, *Geothermobacter,*
456 *Anaeromyxobacter* (Deltaproteobacteria) and *Shewanella* (Gammaproteobacteria) (Weber et al., 2006)
457 comprise less than 0.1% of bacteria detected in the methanic zone (from 185 cm and below), it appears
458 that both the microbial abundance and the Fe(II) concentration peaked at this zone. Cultivation efforts
459 indicated that archaeal methanogens may also play a role in iron reduction within sediments (Sivan et al.,
460 2016). Moreover, the relative abundance of methane-metabolizing archaea was shown to correlate with
461 Fe(II) concentrations in Helgoland muds from the North Sea, where microbial abundance and the Fe(II)
462 concentrations peaked at the methanic zone (Oni et al., 2015), similarly to the Mediterranean sediments.
463 It is possible that methane-metabolizing archaea were involved in the iron reduction in the Mediterranean
464 sediments, as the highest *mcrA* gene copies per gram wet sediment were detected in the SMTZ and in
465 the top of the methanic zone where the Fe(II) concentrations are high. Methanotrophs, such as ANMEs,
466 were found to be involved in iron coupled AOM in marine and freshwater cultures (Scheller et al., 2016;
467 McGlynn et al., 2015; Ettwig et al., 2016; Cai et al., 2018). ANMEs were found here with relatively low
468 frequencies (ANME1, below 1% in most samples, circa 5% in the 185 cm layer), and their role in iron
469 reduction within the Mediterranean sediments remains to be tested.

470 It should be noted that even though the microbial population was tested only on one sediment core that
471 was extracted on January 2017 at Station SG-1, we believe that it represents the general microbial
472 population abundance in the SE Mediterranean continental shelf. In our study, Spearman correlation
473 analysis (Table S2) revealed that bacterial phyla SBR1093 (candidate Phylum), Acidobacteria and
474 Chloroflexi, as well as archaeal Phylum Bathyarchaeota showed significant positive correlation with a
475 Fe(II) concentration in the methanic zone. The Candidate Phylum SBR1093 was firstly identified in
476 phosphate-removing activated sludge from a sequencing batch reactor (Bond et al., 1995), and
477 continuously detected in a short-chain fatty acid rich environment such as wastewater treatment, and
478 marine sediments (Wang et al., 2014). It was thought to be capable of growing autotrophically, but the
479 metabolic capabilities related to iron reduction remain unclear. Strains of Acidobacteria and Chloroflexi
480 phylum were found to be capable of iron reduction (Kawaichi et al., 2013; Kulichevskaya et al., 2014).
481 In addition, members of Acidobacteria were found in iron-coupled AOM enrichment (Beal et al., 2009).
482 The metabolic properties of Subgroup 26 from Acidobacteria and TK10 Class of Chloroflexi are still not
483 known. Bathyarchaeota are globally distributed and account for a considerable fraction of the archaeal
484 communities in the marine sediments, particularly, in the Mediterranean Pleistocene sapropels (Coolen
485 et al., 2002; Zhou et al., 2018). While Bathyarchaeota have diverse metabolic capabilities (Lloyd et al.,
486 2013; Meng et al., 2014; Evans et al., 2015; He et al., 2016; Yu et al., 2018; Feng et al., 2019), their role
487 in iron reduction warrants further studies, as suggested from their high abundance here. Therefore, iron

reduction and methane cycling within the deep methanic zone may be facilitated by an interplay among bacterial and archaeal groups, whose physiology and functions needs further investigation.

5 Conclusions

Our study used combined geochemical and microbial profiles together with slurry incubation experiment to show microbial iron reduction in methanic sediments, and the potential microbial population performing this reduction. The Spearman analysis points out several potential microbial players (both bacterial and archaeal) that correlate to the dissolved Fe(II) profiles (e.g. Bathyarchaeota, Acidobacteria and Chloroflexi). Moreover, our study emphasizes that this methanic iron reduction can occur even in sediments of oligotrophic seas such as the SE Mediterranean. We suggest that the availability of iron minerals for reduction is linked to intensive upward fluxes of methane and high sulfate-AOM rates that may produce available biomass or/and hydrogen, which fuel deeper microbial processes. The deep iron reduction may also be coupled to a cryptic sulfur cycle and iron-coupled AOM.

5 Author contribution

H.V and O.S designed research; B.H and O.S. were the PIs of the cruises; H.V, E.W and L.L performed research and analyzed the data; H.V, O.S, B.H, F.W, M.RB and L.L synthesized the data and wrote the paper.

The authors declare that they have no conflict of interest.

6 Acknowledgments

We thank the captain and crew of the R/V Shikmona and R/V Bat Galim from the Israel Oceanographic and Limnological Research for all their help during field sampling. Many thanks to E. Eliani-Russak for her technical assistance in the lab and to V. Boyko for her help with the reactive iron speciation procedure. We also thank all of Orit's lab member for their help. We would like to thank also to the anonymous reviewers for their helpful and constructive comments. This study was supported by the joint grant of Israel Science Foundation and the National Natural Science Foundation of China (ISF-NSFC) [grant number 31661143022 (FW) and 2561/16 (OS)]. Funding was provided to H. Vigderovich by the Mediterranean Sea Research Center of Israel.

References

Adler, M., Eckert, W. and Sivan, O.: Quantifying rates of methanogenesis and methanotrophy in Lake Kinneret sediments (Israel) using pore-water profiles, Limnol. Oceanogr., 56(4), 1525–1535, doi:10.4319/lo.2011.56.4.1525, 2011.

Almogi-Labin, A., Herut, B., Sandler, A., Gelman, F.: Fast changes at the Israeli continental shelf attributed to the damming of the Nile River., 2009.

Antler, G., Turchyn, A. V, Herut, B. and Sivan, O.: A unique isotopic fingerprint of sulfate-driven anaerobic oxidation of methane, , 43(7), 1–4, doi:10.1130/G36688.1, 2015.

Astrahan, P., Silverman, J., Gertner, Y. and Herut, B.: Spatial distribution and sources of organic matter and pollutants in the SE Mediterranean (Levantine basin) deep water sediments, Mar. Pollut. Bull., 116(1–2), 521–527, doi:10.1016/j.marpolbul.2017.01.006, 2017.

Bar-Or, I., Ben-Dov, E., Kushmaro, A., Eckert, W. and Sivan, O.: Methane-related changes in prokaryotes along geochemical profiles in sediments of Lake Kinneret (Israel), Biogeosciences, 12, 2847–2860, doi:10.5194/bg-12-2847-2015, 2015.

Bar-Or, I., Elvert, M., Eckert, W., Kushmaro, A., Vigderovich, H., Zhu, Q., Ben-Dov, E. and Sivan, O.: Iron-Coupled Anaerobic Oxidation of Methane Performed by a Mixed Bacterial-Archaeal Community Based on Poorly Reactive Minerals, Environ. Sci. Technol., 51, 12293–12301, doi:10.1021/acs.est.7b03126, 2017.

Bareket, M. M., Bookman, R., Katsman, R., de Stigter, H. and Herut, B.: The role of transport processes of particulate mercury in modifying marine anthropogenic secondary sources, the case of Haifa bay, Israel, Mar. Pollut. Bull., 105(1), 286–291, doi:10.1016/j.marpolbul.2016.02.014, 2016.

Beal, E. J., House, C. H. and Orphan, V. J.: Manganese-and Iron-Dependent Marine Methane Oxidation, Science, 325(5937), 184–187, doi:10.1126/science.1169984, 2009.

Boetius, A., Ravenschlag, K., Schubert, C. J., Rickert, D., Widdel, F., Gieseke, A., Amann, R., Jùrgensen, B. B., Witte, U. and Pfannkuche, O.: A marine microbial consortium apparently mediating anaerobic oxidation of methane, Lett. to Nat., 407(October), 623–626, 2000.

Bond, D. R., Lovley, D. R.: Reduction of Fe (III) oxide by methanogens in the presence and absence of extracellular quinones, Environ. Microbiol., 4(2), 115–124,doi: 10.1046/j.1462-2920.2002.00279.x, 2002.

Bond, P. L., Hugenholtz, P., Keller, J. and Blackall, L. L.: Bacterial Community Structures of Phosphate-Removing and Non-Phosphate-Removing Activated Sludges from Sequencing Batch Reactors, , 61(5), 1910–1916, 1995.

Bottrell, S. H., Parkes, R. J., Cragg, B. a. and Raiswell, R.: Isotopic evidence for anoxic pyrite oxidation and stimulation of bacterial sulphate reduction in marine sediments, J. Geol. Soc. London., 157(4), 711–714, doi:10.1144/jgs.157.4.711, 2000.

Bray, M. S., Jieying, W., Reed, B. C., Kretz, C. B., Belli, K. M., Simister, R. L., Henny, C., Stewart, F. J., DiChristina, T. J., Brandes, J. A., Fowle, D. A., Crowe, S. A. and Glass, J. B.: Shifting microbial communities sustain multi-year iron reduction and methanogenesis in ferruginous sediment incubations, Geobiology, doi: 10.1101/087783., 2018.

Brunner, B., Arnold, G. L., Røy, H., Müller, I. A. and Jørgensen, B. B.: Off Limits : Sulfate below the Sulfate-Methane Transition, , 4(July), 1–16, doi:10.3389/feart.2016.00075, 2016.

Buongiorno, J., Turner, S., Webster, G., Asai, M., Shumaker, A. K., Roy, T., Weightman, A., Schippers, A. and Lloyd, K. G.: Interlaboratory quantification of Bacteria and Archaea in deeply buried

558 sediments of the Baltic Sea (IODP Expedition 347), FEMS Microbiol. Ecol., (93), 1–16,
559 doi:10.1093/femsec/fix007, 2017.

560 Cai, C., Leu, A. O., Jianhua, G. X., Yuexing, G., Zhao, F. J. and Tyson, G. W.: A methanotrophic
561 archaeon couples anaerobic oxidation of methane to Fe (III) reduction, ISME J., 8, 1929-1939,
562 doi:10.1038/s41396-018-0109-x, 2018.

563 Caporaso, J. G., Kuczynski, J., Stombaugh, J., Bittinger, K., Bushman, F. D., Costello, E. K., Fierer,
564 N., Peña, A. G., Goodrich, J. K., Gordon, J. I., Huttley, G. A., Kelley, S. T., Knights, D., Koenig, J. E.,
565 Ley, R. E., Lozupone, C. A., McDonald, D., Muegge, B. D., Pirrung, M., Reeder, J., Sevinsky, J. R.,
566 Turnbaugh, P. J., Walters, W. A., Widmann, J., Yatsunenko, T., Zaneveld, J. and Knight, R.: QIIME
567 allows analysis of high-throughput com- munity sequencing data., Nat. Methods, (7), 335–336,
568 doi:10.1038/nmeth.f.303, 2010.

569 Chen, W. H., Chen, S. Y., Kumar Khanal, S. and Sung, S.: Kinetic study of biological hydrogen
570 production by anaerobic fermentation, Int. J. Hydrogen Energy, 31(15), 2170–2178,
571 doi:10.4304/jcp.6.4.740-746, 2006.

572 Cline, J. D.: Spectrophotometric determination of hydrogen sulfide in natural waters, Limnol.
573 Oceanogr., 454–458, doi:https://doi.org/10.4319/lo.1969.14.3.0454, 1969.

574 Conrad, R.: Contribution of hydrogen to methane production and control of hydrogen concentrations in
575 methanogenic soils and sediments, FEMS Microbiol. Ecol., 28(3), 193–202, 1999.

576 Coolen, M. J. L., Cypionka, H., Sass, A. M., Sass, H. and Overmann, J.: Ongoing modification of
577 Mediterranean pleistocene sapropels mediated by prokaryotes, Science (80-.)., 296(June), 2407–2411,
578 doi:10.1126/science.1071893, 2002.

579 Crowe, S. A., Katsev, S., Leslie, K., Sturm, A., Magen, C., Nomosatryo, S., Pack, M. A., Kessler, J. D.,
580 Reeburgh, W. S., Robert S, J. A., Gonzalez, L., Douglas Haffner, G., Mucci, A., Sundby, B. and Fowle,
581 D. .: The methane cycle in ferruginous Lake Matano, Geobiology, 9, 61–78, doi:10.1111/j.1472-
582 4669.2010.00257.x, 2011.

583 Egger, M., Rasigraf, O., Sapart, C. J., Jilbert, T., Jetten, M. S. M., Röckmann, T., Van Der Veen, C.,
584 Bânda, N., Kartal, B., Ettwig, K. F. and Slomp, C. P.: Iron-mediated anaerobic oxidation of methane in
585 brackish coastal sediments, Environ. Sci. Technol., 49(1), 277–283, doi:10.1021/es503663z, 2014.

586 Egger, M., Kraal, P., Jilbert, T., Sulu-Gambari, F., Sapart, C. J., Röckmann, T. and Slomp, C. P.:
587 Anaerobic oxidation of methane alters diagenetic records of sulfur, iron and phosphorus in Black Sea
588 sediments, Biogeosciences Discuss., (March), 1–39, doi:10.5194/bg-2016-64, 2016.

589 Egger, M., Hagens, M., Sapart, C. J., Dijkstra, N., van Helmond, N. A. G. M., Mogollón, J. M.,
590 Risgaard-Petersen, N., van der Veen, C., Kasten, S., Riedinger, N., Böttcher, M. E., Röckmann, T.,
591 Jørgensen, B. B. and Slomp, C. P.: Iron oxide reduction in methane-rich deep Baltic Sea sediments,
592 Geochim. Cosmochim. Acta, 207, 256–276, doi:10.1016/j.gca.2017.03.019, 2017.

Emerson, S., Jahnke, R., Bender, M., Froelich, P. and Klinkhammer, G.: Early diagenesis in sediments from the eastern equatorial pacific, i. pore water nutrient and carbonate results, Earth Planet. Sci. Lett., 49, doi:https://doi.org/10.1016/0012-821X(80)90150-8, 1980.

Ettwig, K. F., Zhu, B., Speth, D., Keltjens, J. T., Jetten, M. S. M. and Kartal, B.: Archaea catalyze iron-dependent anaerobic oxidation of methane, Proc. Natl. Acad. Sci., 113(45), 12792–12796, doi:10.1073/pnas.1609534113, 2016a.

Ettwig, K. F., Zhu, B., Speth, D., Keltjens, J. T., Jetten, M. S. M. and Kartal, B.: Archaea catalyze iron-dependent anaerobic oxidation of methane, Proc. Natl. Acad. Sci., 113(45), 12792–12796, doi:10.1073/pnas.1609534113, 2016b.

Evans, P. N., Parks, D. H., Chadwick, G. L., Robbins, S. J., Orphan, V. J., Golding, S. D. and Tyson, G. W.: Methane metabolism in the archaeal phylum Bathyarchaeota revealed by genome-centric metagenomics, Science, 350(6259), 434–438, doi:10.1126/science.aac7745, 2015.

Feng, X., Wang, Y., Zubin, R. and Wang, F.: Core Metabolic Features and Hot Origin of Bathyarchaeota, Engineering, doi:10.1016/j.eng.2019.01.011, 2019.

Froelich, P. N., Klinkhammer, G. P., Bender, M. L., Luedtke, N. A., Heath, G. R., Cullen, D., Dauphin, P., Hammond, D., Hartman, B. and Maynard, V.: Early oxidation of organic matter in pelagic sediments of the eastern equatorial Atlantic: Suboxic diagenesis, Geochim. Cosmochim. Acta, 43, 1075–1090, doi:https://doi.org/10.1016/0016-7037(79)90095-4, 1979.

He, Y., Li, M., Perumal, V., Feng, X., Fang, J., Xie, J., Sievert, S. M. and Wang, F.: Genomic and enzymatic evidence for acetogenesis among multiple lineages of the archaeal phylum Bathyarchaeota widespread in marine sediments, Nat. Microbiol., (April), 1–9, doi:10.1038/nmicrobiol.2016.35, 2016.

Herut, B., Almogi-Labin, A., Jannink, N. and Gertman, I.: The seasonal dynamics of nutrient and chlorophyll a concentrations on the SE Mediterranean shelf-slope, Oceanol. Acta, 23(7), 771–782, doi:10.1016/S0399-1784(00)01118-X, 2000.

Hinrichs, K., Hayes, J. M. and Sylva, S. P.: Methane-consuming archaebacteria in marine sediments, Lett. to Nat., 398(April), 802–805, 1999.

Holmkvist, L., Ferdelman, T. G. and Jørgensen, B. B.: A cryptic sulfur cycle driven by iron in the methane zone of marine sediment (Aarhus Bay, Denmark), Geochim. Cosmochim. Acta, 75(12), 3581–3599, doi:10.1016/j.gca.2011.03.033, 2011.

Iversen, N. and Jorgensen, B. B.: Anaerobic methane oxidation rates at the sulfate-methane transition in marine sediments from Kattegat and Skagerrak (Denmark), Limnol. Oceanogr., 1983(5), 944–955, 1985.

Jorgensen, B. B., Bottcher, M. E., Luschen, H., Neretin, L. N. and Volkov, I. I.: Anaerobic methane oxidation and a deep H_2S sink generate isotopically heavy sulfides in Black Sea sediments, Geochim. Cosmochim. Acta, 68(9), 2095–2118, doi:10.1016/j.gca.2003.07.017, 2004.

628 Kawaichi, S., Ito, N., Kamikawa, R., Sugawara, T., Yoshida, T. and Sako, Y.: Ardenticatena maritima
629 gen. nov., sp. nov., a ferric iron- and nitrate-reducing bacterium of the phylum 'Chloroflexi' isolated
630 from an iron-rich coastal hydrothermal field, and description of Ardenticatenia classis nov., Int. J. Syst.
631 Evol. Microbiol., (63), 2992–3002, doi:10.1099/ijs.0.046532-0, 2013.

632 Knittel, K. and Boetius, A.: Anaerobic Oxidation of Methane : Progress with an Unknown Process,
633 Annu. Rev. Microbiol., 63, 311-334, doi:10.1146/annurev.micro.61.080706.093130, 2009.

634 Kulichevskaya, I. S., Suzina, N. E., Rijpstra, W. I. C., Dedysh, S. N. and Damste, J. S. S.: a facultative
635 anaerobe capable of dissimilatory iron reduction from subdivision 3 of the Acidobacteria, Int. J. Syst.
636 Evol. Microbiol., (64), 2857–2864, doi:10.1099/ijs.0.066175-0, 2014.

637 Li, Y., Yu, S., Strong, J. and Wang, H.: Are the biogeochemical cycles of carbon , nitrogen , sulfur ,
638 and phosphorus driven by the " Fe III – Fe II redox wheel " in dynamic redox environments ?, J. soils
639 sediments, 12(5), 683–693, doi:10.1007/s11368-012-0507-z, 2012.

640 Lilley, M. D., Baross, J. A. and Gordon, L. I.: Dissolved hydrogen and methane in Saanich Inlet,
641 British Columbia, Deep Sea Res. Part A, Oceanogr. Res. Pap., 29(12), 1471–1484, doi:10.1016/0198-
642 0149(82)90037-1, 1982.

643 Liu, D., Dong Hailiang, H., Bishop, M. E., Wang, H., Agrawal, A., Tritschler, S., Eberl, D. D. and Xie,
644 S.: Reduction of structural Fe(III) in nontronite by methanogen Methanosarcina barkeri, Geochim.
645 Cosmochim. Acta, 75(4), 1057–1071, doi:10.1016/j.gca.2010.11.009, 2011.

646 Lloyd, K. G., Schreiber, L., Petersen, D. G., Kjeldsen, K. U., Lever, M. A., Steen, A. D., Stepanauskas,
647 R., Richter, M., Kleindienst, S., Lenk, S., Schramm, A. and Jørgensen, B. B.: Predominant archaea in
648 marine sediments degrade detrital proteins, Nature, 496(7444), 215–218, doi:10.1038/nature12033,
649 2013.

650 Lovley, Derek R. and Goodwin, S.: Hydrogen concentrations as an indicator of the predominant
651 terminal electron-accepting reactions in aquatic sediments, Geochim. Cosmochim. Acta, 52, 2993–
652 3003, doi:10.1016/0016-7037(88)90163-9, 1988.

653 Lovley, D. R.: Dissimilatory Fe(III) and Mn(IV) reduction., Microbiol. Rev., 55(2), 259–287, 1991.

654 Lovley, D. R. and Phillips, E. J.: Novel mode of microbial energy metabolism: organic carbon
655 oxidation coupled to dissimilatory reduction of iron or manganese., Appl. Environ. Microbiol., 54(6),
656 1472–1480, doi:10.1103/PhysRevLett.50.1998, 1988.

657 Lovley, D. R. and Phillips, E. J. P.: Organic matter mineralization with reduction of ferric iron in
658 anaerobic sediments., Appl. Environ. Microbiol., 51(4), 683–689, doi:10.1080/01490458709385975,
659 1986.

660 Lovley, D. R., Coates, J. D., BluntHarris, E. L., Phillips, E. J. P. and Woodward, J. C.: Humic
661 substances as electron acceptors for microbial respiration, Nature, 382(6590), 445–448,
662 doi:10.1038/382445a0, 1996.

März, C., Hoffmann, J., Bleil, U., Lange, G. J. De and Kasten, S.: Diagenetic changes of magnetic and geochemical signals by anaerobic methane oxidation in sediments of the Zambezi deep-sea fan (SW Indian Ocean), Mar. Geol., 255(3–4), 118–130, doi:10.1016/j.margeo.2008.05.013, 2008.

März, C., Riedinger, N., Sena, C. and Kasten, S.: Phosphorus dynamics around the sulphate-methane transition in continental margin sediments : Authigenic apatite and Fe (II) phosphates, Mar. Geol., 404(July), 84–96, doi:10.1016/j.margeo.2018.07.010, 2018.

McGlynn, S. E., Chadwick, G. L., Kempes, C. P. and Orphan, V. J.: Single cell activity reveals direct electron transfer in methanotrophic consortia, Nature, 526(7574), 531–535, doi:10.1038/nature15512, 2015.

Meng, J., Xu, J., Qin, D., He, Y., Xiao, X. and Wang, F.: Genetic and functional properties of uncultivated MCG archaea assessed by metagenome and gene expression analyses, ISME J., 8(3), 650–9, doi:10.1038/ismej.2013.174, 2014.

Milkov, A. V: Global estimates of hydrate-bound gas in marine sediments : how much is really out there ?, Earth-Science Rev., 66, 183–197, doi:10.1016/j.earscirev.2003.11.002, 2004.

Milkov, A. V and Sassen, R.: Economic geology of offshore gas hydrate accumulations and provinces, Mar. Pet. Geol., 19, 1–11, doi:doi.org/10.1016/S0264-8172(01)00047-2, 2002.

Mountfort, D. O. and Asher, R. A.: Role of Sulfate Reduction Versus Methanogenesis in Terminal Carbon Flow in Polluted Intertidal Sediment of Waimea Inlet, Nelson, New Zealand, Appl. Environ. Microbiol., 42(2), 252–258, doi: 0099-2240/81/080252-07$02.00/0, 1981.

Mountfort, D. O., Asher, R. a, Mays, E. L. and Tiedje, J. M.: Carbon and electron flow in mud and sandflat intertidal sediments at delaware inlet, nelson, new zealand., Appl. Environ. Microbiol., 39(4), 686–94 doi: 0099-2240/80/04-0686/09$02.00/0, 1980.

Moutin, T. and Raimbault, P.: Primary production , carbon export and nutrients availability in western and eastern Mediterranean Sea in early summer 1996 (MINOS cruise), J. Mar. Syst., 34, 273–288, doi: doi.org/10.1016/S0924-7963(02)00062-3, 2002.

Nir, Y.: Recent sediments of the Israel Mediterranean continental shelf and slope, University of Gothenburg. http://hdl.handle.net/2077/13267, 1984.

Niu, M., Fan, X., Zhuang, G., Liang, Q. and Wang, F.: Methane-metabolizing microbial communities in sediments of the Haima cold seep area , northwest slope of the South China Sea, FEMS Microbiol. Ecol., (March), 1–13, doi:10.1093/femsec/fix101, 2017.

Nordi, K. Á., Thamdrup, B. and Schubert, C. J.: Anaerobic oxidation of methane in an iron-rich Danish freshwater lake sediment, Limnol. Oceanogr., 58(2), 546–554, doi:10.4319/lo.2013.58.2.0546, 2013.

Novelli, P. C., Scranton, M. I. and Michener, R. H.: Hydrogen Distributions in Marine Sediments Hydrogen distributions, , 32(3), 565–576, doi:10.4319/lo.1987.32.3.0565, 1987.

Nusslein, B., Eckert, W. and Conrad, R.: Stable isotope biogeochemistry of methane formation in profundal sediments of Lake Kinneret (Israel), , 48(4), 1439–1446, doi:10.4319/lo.2003.48.4.1439, 2003.

Oni, O., Miyatake, T., Kasten, S., Richter-Heitmann, T., Fischer, D., Wagenknecht, Laura Kulkarni, A., Blumers, M., Shylin, S. I., Ksenofontov, Vadim Costa, B. F. O., Klingelhöfer, G. and Friedrich, M. W.: Distinct microbial populations are tightly linked to the profile of dissolved iron in the methanic sediments of the Helgoland mud area , North Sea, Front. Microbiol., 6(May), 1–15, doi:10.3389/fmicb.2015.00365, 2015.

Orphan, V. J., House, C. H. and Hinrichs, K.: Methane-Consuming Archaea Revealed by Directly Coupled Isotopic and Phylogenetic Analysis, Science (80-.)., 293(July), 484–488, doi:10.1126/science.1061338, 2001.

Paull, C. K., Normark, W. R., Ussler, W., Caress, D. W. and Keaten, R.: Association among active seafloor deformation , mound formation , and gas hydrate growth and accumulation within the seafloor of the Santa Monica Basin , offshore California, Mar. Geol., 250, 258–275, doi:10.1016/j.margeo.2008.01.011, 2008.

Poulton, S. W. and Canfield, D. E.: Development of a sequential extraction procedure for iron: Implications for iron partitioning in continentally derived particulates, Chem. Geol., 214(3–4), 209–221, doi:10.1016/j.chemgeo.2004.09.003, 2005.

Riedinger, N., Formolo, M. J., Lyons, T. W., Henkel, S., Beck, A. and Kasten, S.: An inorganic geochemical argument for coupled anaerobic oxidation of methane and iron reduction in marine sediments, Geobiology, 12(2), 172–181, doi:10.1111/gbi.12077, 2014.

Riedinger, N., Brunner, B., Krastel, S., Arnold, G. L., Wehrmann, L. M., Formolo, M. J., Beck, A., Bates, S. M., Henkel, S., Kasten, S. and Lyons, T. W.: Sulfur Cycling in an Iron Oxide-Dominated , Dynamic Marine Depositional System : The Argentine Continental Margin, Front. earth Sci., 5(May), doi:10.3389/feart.2017.00033, 2017.

Roden, E. E.: Fe(III) Oxide Reactivity Toward Biological versus Chemical Reduction, Environ. Sci. Technol., 37(7), 1319–1324, doi:10.1021/es026038o, 2003.

Roden, E. E.: Geochemical and microbiological controls on dissimilatory iron reduction, Comptes Rendus - Geosci., 338(6–7), 456–467, doi:10.1016/j.crte.2006.04.009, 2006.

Roden, E. E. and Wetzel, R. G.: Organic carbon oxidation and suppression of methane production by microbial Fe(III) oxide reduction in vegetated and unvegetated freshwater wetland sediments, Limnol. Oceanogr., 41(8), 1733–1748, doi:10.4319/lo.1996.41.8.1733, 1996.

Roden, E. E. and Wetzel, R. G.: Kinetics of microbial Fe (III) oxide reduction in freshwater wetland sediments, Limnol. Ocean., 47(1), 198–211, doi:10.4319/lo.2002.47.1.0198, 2002.

Rooze, J., Egger, M., Tsandev, I. and Slomp, C. P.: Iron-dependent anaerobic oxidation of methane in

732 coastal surface sediments: potential controls and impact, Limnol. Oceanogr., (1),
733 doi:10.1002/lno.10275, 2016.

734 Salem, D. M. S. A., Khaled, A. and Nemr, A. El: Assessment of pesticides and polychlorinated
735 biphenyls (PCBs) in sediments of the Egyptian Mediterranean Coast, Egypt. J. Aquat. Res., 39(3),
736 141–152, doi:10.1016/j.ejar.2013.11.001, 2013.

737 Sandler, A. and Herut, B.: Composition of clays along the continental shelf off Israel: Contribution of
738 the Nile versus local sources, Mar. Geol., 167(3–4), 339–354, doi:10.1016/S0025-3227(00)00021-9,
739 2000.

740 Schattner, U., Lazar, M., Harari, D. and Waldmann, N.: Active gas migration systems offshore northern
741 Israel, first evidence from seafloor and subsurface data, Cont. Shelf Res., 48, 167–172,
742 doi:10.1016/j.csr.2012.08.003, 2012.

743 Scheller, S., Yu, H., Chadwick, G. L., McGlynn, S. E. and Orphan, V. J.: Artificial electron acceptors
744 decouple archaeal methane oxidation from sulfate reduction, Science, 351(6274), 1754–1756,
745 doi:10.1126/science.aad7154, 2016.

746 Segarra, K. E. a, Comerford, C., Slaughter, J. and Joye, S. B.: Impact of electron acceptor availability
747 on the anaerobic oxidation of methane in coastal freshwater and brackish wetland sediments, Geochim.
748 Cosmochim. Acta, 115, 15–30, doi:10.1016/j.gca.2013.03.029, 2013.

749 Sela-Adler, M., Herut, B., Bar-Or, I., Antler, G., Eliani-Russak, E., Levy, E., Makovsky, Y. and Sivan,
750 O.: Geochemical evidence for biogenic methane production and consumption in the shallow sediments
751 of the SE Mediterranean shelf (Israel), Cont. Shelf Res., 101, 117–124, doi:10.1016/j.csr.2015.04.001,
752 2015.

753 Sivan, O., Schrag, D. P. and Murray, R. W.: Rates of methanogenesis and methanotrophy in deep-sea
754 sediments, Geobiology, 5(2), 141–151, doi:10.1111/j.1472-4669.2007.00098.x, 2007.

755 Sivan, O., Adler, M., Pearson, A., Gelman, F., Bar-Or, I., John, S. G. and Eckert, W.: Geochemical
756 evidence for iron-mediated anaerobic oxidation of methane, Limnol. Oceanogr., 56(4), 1536–1544,
757 doi:10.4319/lo.2011.56.4.1536, 2011.

758 Sivan, O., Antler, G., Turchyn, A. V., Marlow, J. J. and Orphan, V. J.: Iron oxides stimulate sulfate-
759 driven anaerobic methane oxidation in seeps, Proc. Natl. Acad. Sci., 111, E4139–E4147,
760 doi:10.1073/pnas.1412269111, 2014.

761 Sivan, O., Shusta, S. and Valentine, D. L.: Methanogens rapidly transition from methane production to
762 iron reduction, Geobiology, 190–203, doi:10.1111/gbi.12172, 2016.

763 Slomp, C. P., Mort, H. P., Jilbert, T., Reed, D. C., Gustafsson, B. G. and Wolthers, M.: Coupled
764 Dynamics of Iron and Phosphorus in Sediments of an Oligotrophic Coastal Basin and the Impact of
765 Anaerobic Oxidation of Methane, PLoS One, 8(4), doi:10.1371/journal.pone.0062386, 2013.

766 Song, Z., Wang, F., Zhi, X., Chen, J., Zhou, E., Liang, F., Xiao, X., Tang, S., Jiang, H., Zhang, C. L.,

Dong, H. and Li, W.: Bacterial and archaeal diversities in Yunnan and Tibetan hot springs , China, , 15, 1160–1175, doi:10.1111/1462-2920.12025, 2013.

Stookey, L. L.: Ferrozine-a new spectrophotometric reagent for iron, Anal. Chem., 42(7), 779–781, doi:10.1021/ac60289a016, 1970.

Tan, S., Liu, J., Fang, Y., Hedlund, B. P., Lian, Z., Li, L. H. J., Li, L. H. W., Dong, H. J. H. and Shu, W.: Insights into ecological role of a new deltaproteobacterial order Candidatus Acidulodesulfobacterales by metagenomics and metatranscriptomics, ISME J., doi:10.1038/s41396-019-0415-y, 2019.

Treude, T., Krause, S., Maltby, J., Dale, A. W., Coffin, R. and Hamdan, L. J.: Sulfate reduction and methane oxidation activity below the sulfate-methane transition zone in Alaskan Beaufort Sea continental margin sediments: Implications for deep sulfur cycling, Geochim. Cosmochim. Acta, 144, 217–237, doi:10.1016/j.gca.2014.08.018, 2014.

Walters, W., Hyde, E. R., Berg-lyons, D., Ackermann, G., Humphrey, G., Parada, A., Gilbert, J. A. and Jansson, J. K.: Transcribed Spacer Marker Gene Primers for Microbial Community Surveys, Am. Soc. Microbiol., 1(1), 1–10, doi:10.1128/mSystems.00009-15, 2015.

Wang, Z., Guo, F., Liu, L. and Zhang, T.: Evidence of Carbon Fixation Pathway in a Bacterium from Candidate Phylum SBR1093 Revealed with Genomic Analysis, PLoS One, 9(10), doi:10.1371/journal.pone.0109571, 2014.

Weber, K. A., Urrutia, M. M., Churchill, P. F., Kukkadapu, R. K. and Roden, E. E.: Anaerobic redox cycling of iron by freshwater sediment microorganisms, Environ. Microbiol., 8(1), 100–113, doi:10.1111/j.1462-2920.2005.00873.x, 2006.

Whiticar, M. J.: Carbon and hydrogen isotope systematics of bacterial formation and oxidation of methane, Chem. Geol., 161(1–3), 291–314, doi:10.1016/S0009-2541(99)00092-3, 1999.

Wurgaft, E., Findlay, A. J., Vigderovich, H., Herut, B. and Sivan, O.: Sulfate reduction rates in the sediments of the Mediterranean continental shelf inferred from combined dissolved inorganic carbon and total alkalinity profiles, Mar. Chem., (February), 1–11, doi:10.1016/j.marchem.2019.03.004, 2019.

Yan, Z., Joshi, P., Gorski, C. A. and Ferry, J. G.: A biochemical framework for anaerobic oxidation of methane driven by Fe(III)-dependent respiration, Nat. Commun., (Iii), 1–9, doi:10.1038/s41467-018-04097-9, 2018.

Yu, T., Wu, W., Liang, W., Alexander, M. and Hinrichs, K.: Growth of sedimentary Bathyarchaeota on lignin as an energy source, Proc. Natl. Acad. Sci., 115(23), 6022–6027, doi:10.1073/pnas.1718854115, 2018.

Zehnder, a. J. B. and Brock, T. D.: Anaerobic methane oxidation: Occurrence and ecology, Appl. Environ. Microbiol., 39(1), 194–204 http://aem.asm.org/content/39/1/194, 1980.

Zhang, C. L. and Lanoil, B.: Geomicrobiology and biogeochemistry of gas hydrates and cold seeps,

802 Chemocal Geol., 205, 187–194, doi:10.1016/j.chemgeo.2004.01.001, 2004.

803 Zhang, J., Dong, H., Liu, D., Fischer, T. B., Wang, S. and Huang, L.: Microbial reduction of Fe(III) in
804 illite–smectite minerals by methanogen Methanosarcina mazei, Chem. Geol., 292–293, 35–44,
805 doi:10.1016/j.chemgeo.2011.11.003, 2012.

806 Zhang, J., Dong, H., Liu, D. and Agrawal, A.: Microbial reduction of Fe(III) in smectite minerals by
807 thermophilic methanogen Methanothermobacter thermautotrophicus, Geochim. Cosmochim. Acta, 106,
808 203–215, doi:10.1016/j.gca.2012.12.031, 2013.

809 Zhou, Z., Pan, J., Wang, F., Gu, J. and Li, M.: Bathyarchaeota : globally distributed metabolic
810 generalists in anoxic environments, FEMS Microbiol. Rev., (May), 639–655,
811 doi:10.1093/femsre/fuy023, 2018.

812

813

814 **Table 1**: Sampling details: dates, water depths and locations of the cores.

Date	station	water depth (m)	Latitude	Longtitude
August 14, 2013	PC-5	87	32°55.47'	34°54.01'
	PC-3	81	32°55.29'	34°54.14'
February 6, 2014	PC-3	82	32°55.30'	34°54.14'
January, 2015	PC-3	82	32°55.30'	34°54.14'
June 9, 2015	SG-1	89	32°57.87'	34°55.30'
September 17, 2015	SG-1	84	32°57.91'	34°55.27'
January 24, 2017	SG-1	85	32°57.51'	34°55.15'

815

816 **Table 2**: Summary of reactive iron extraction procedure (after Poulton and Canfield, 2005).

Extractant	Target compounds	Analyzed species	Formula	Shaking time (h)
Magnesium chloride	Ion-exchangeble Fe(II)	Adsorbed ferrous iron	Fe^{2+}	2
Sodium acetate	Iron carbonates	Siderite Ankerite	$FeCO_3$ $Ca(Fe^{+2},Mg^{+2},Mn^{+2})(CO_3)_2$	24
Hydroxylamine hydrochloride	"Easily reducible" Iron(hydr)oxides	Ferrihydrite, Lepidicrocite	$Fe^{3+}{}_2O_3*0.5(H_2O)$ γ-FeOOH	48
Sodium dithionite	"Reducible" oxides	Goethite, Hematite, Akageneite	α-FeOOH Fe_2O_3 β-FeOOH	2
Ammonium oxalate	Poorly crystalline	Magnetite	Fe_3O_4	6

817

818 **Figures captions:**

Figure 1: A map of the study area in the SE Mediterranean with the location of the three sampled stations: SG-1, PC-3 and PC-5 (after Wurgaft et al., 2019).

819 **Figure 2**: Geochemical pore-water profiles of sediment cores collected from Station SG-1 (top) and Station PC-3 (bottom) in the SE Mediterranean. The profiles are divided roughly to three zones according to the dominant processes: upper microbial iron and sulfate reduction, sulfate-methane transition zone (SMTZ), and the methanic zone at the deep part. The dashed line in the CH_4 graph at SG-1 station represents the CH_4 saturation value in the pore-water. The following iron minerals profiles in stations SG-1 and PC-3 are from the September 2015 and January 2015 cruise (respectively): siderite, ankerite (●), ferrihydrite, lepidocrocite (■) goethite, hematite, akaganeite (▲), magnetite (▼), pyrite (◆) and total reactive iron (⬣). The error bars for CH_4 are presented where duplicate samples were collected. The error bars for Fe(II), $\delta^{13}C_{DIC}$ and H_2 are presented where measurement repetition of each sample was taken (at least twice). The analytical errors were smaller than the symbols. BC-Box core.

Figure 3: Sedimentary depth profiles of bacterial and archaeal 16S rRNA and mcrA functional genes of Station SG-1 from January 2017, divided to three zones (as described in figure 2). Triplicates were produced from each sample with error bars smaller than the symbols.

Figure 4: Phyla level classification of bacterial (a) and archaeal (b) diversity in the sediments of Station SG-1 from January 2017.

Figure 5: Dissolved Fe(II) results of the sediment slurry incubation experiment. The sediment was collected from Station SG-1 on January 2017 from sediment depth of 265-285 cm. The error bars were smaller than the symbol.

Figure 6: The relationship between dissolved Fe(II) concentrations and methane concentrations in zone 3 of (a) Station SG-1 and (b) Station PC-3. An inverse association is observed between the two species, suggesting a relationship of competition or iron-coupled AOM.

Figures:

Figure 1

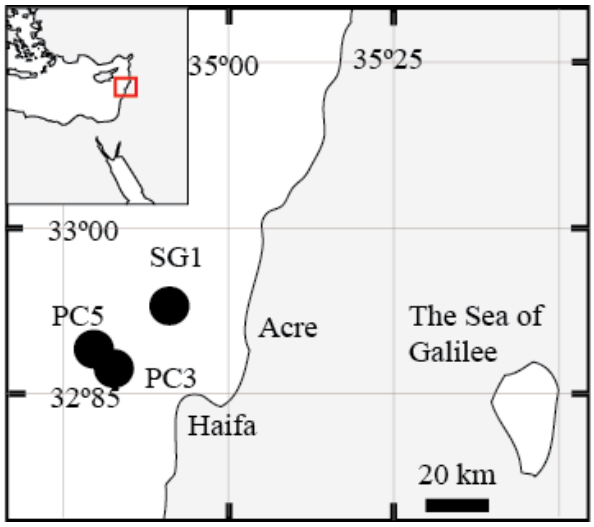

852 **Figure 2**

853

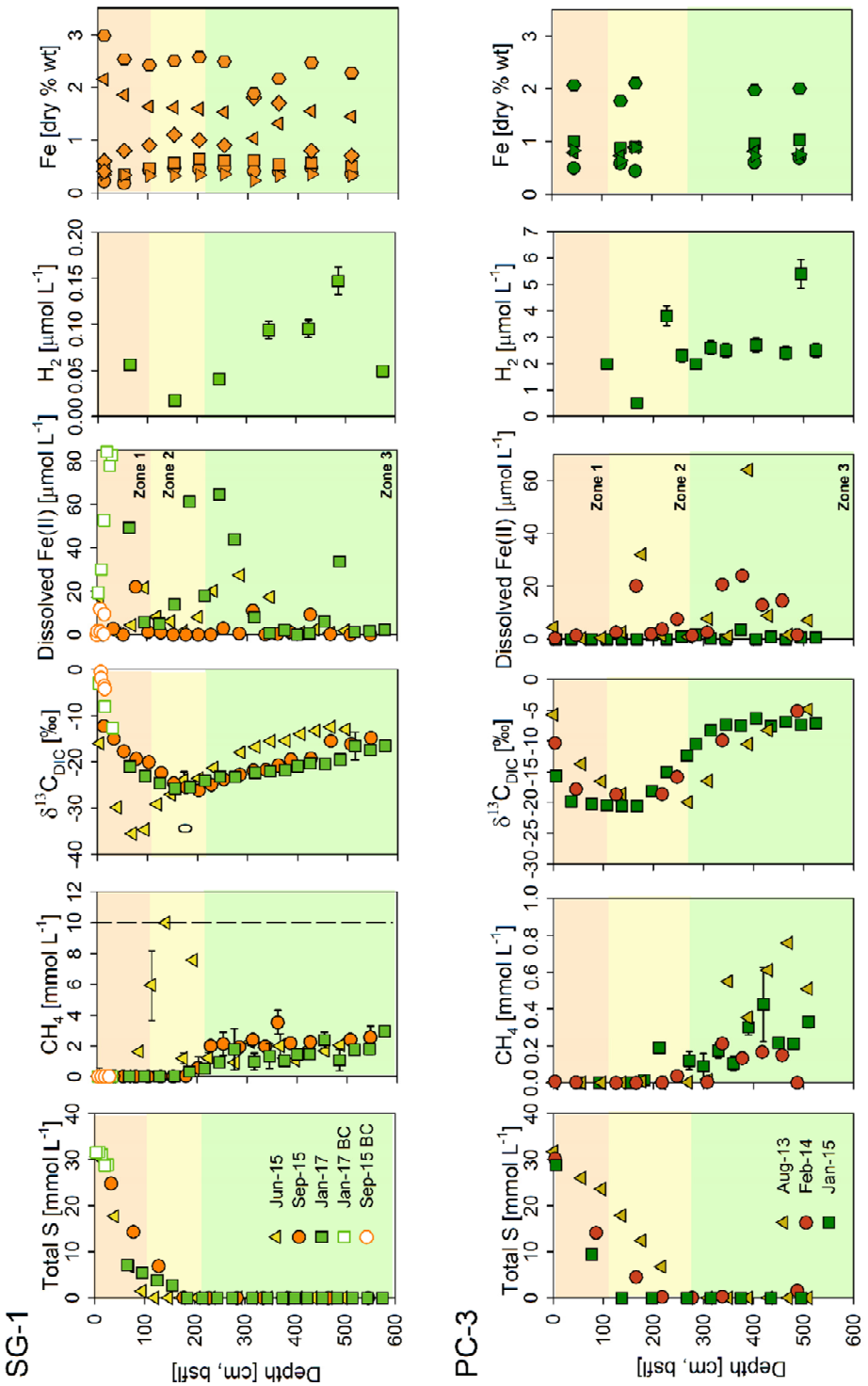

855 **Figure 3**

856

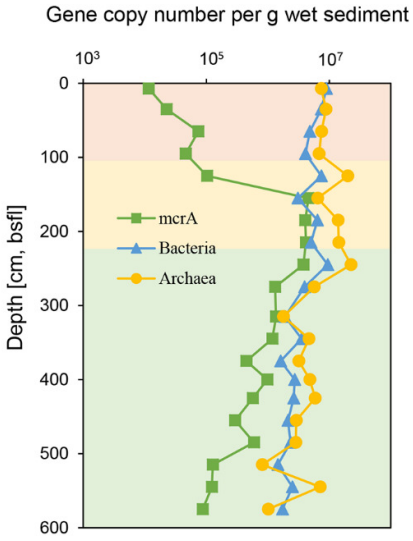

Figure 4

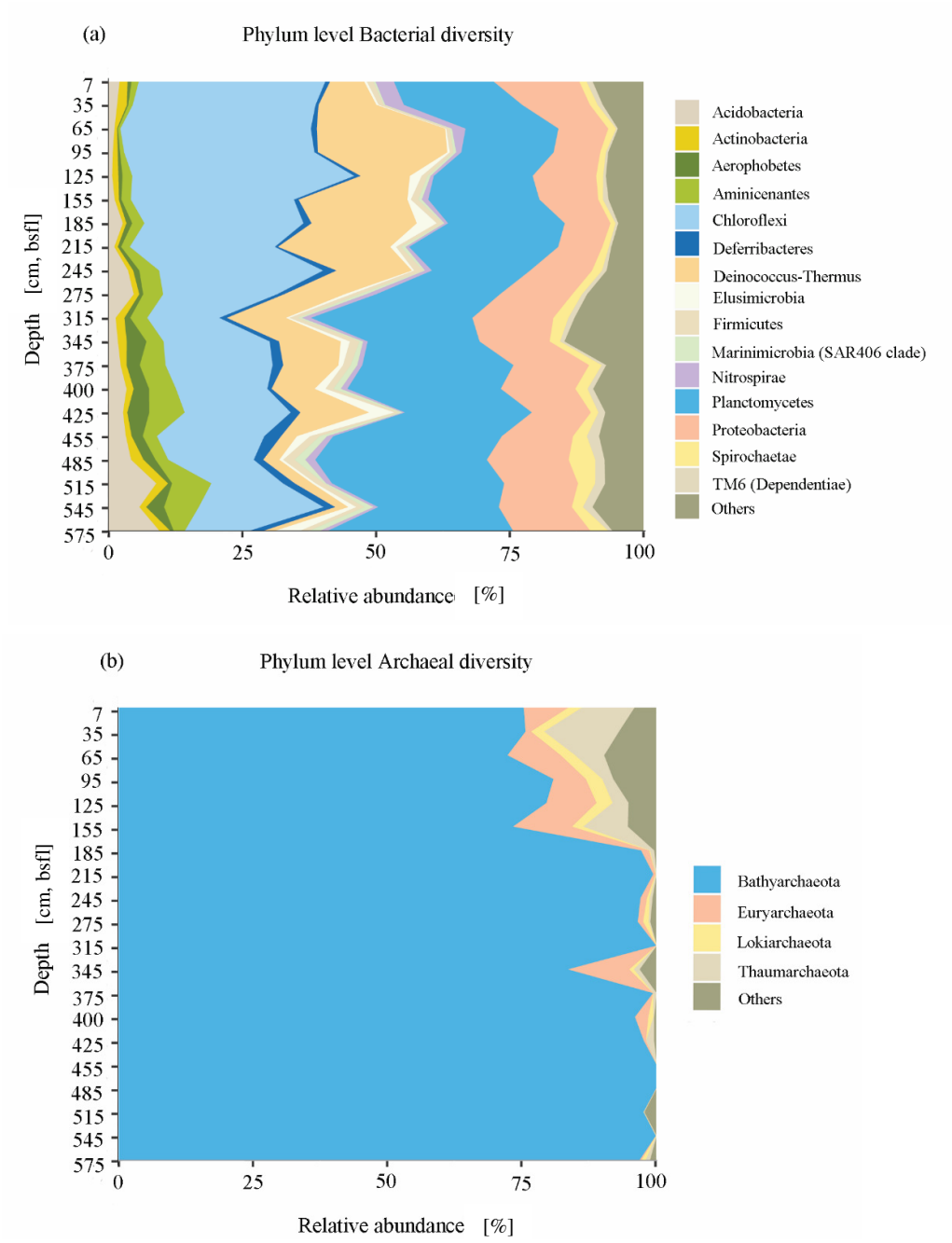
(a)
Phylum level Bacterial diversity
Depth [cm, bsfl]
7
35
65
95
125
155
185
215
245
275
315
345
375
400
425
455
485
515
545
575
0
25
50
75
100
Relative abundance [%]
Acidobacteria
Actinobacteria
Aerophobetes
Aminicenantes
Chloroflexi
Deferribacteres
Deinococcus-Thermus
Elusimicrobia
Firmicutes
Marinimicrobia (SAR406 clade)
Nitrospirae
Planctomycetes
Proteobacteria
Spirochaetae
TM6 (Dependentiae)
Others
(b)
Phylum level Archaeal diversity
Depth [cm, bsfl]
7
35
65
95
125
155
185
215
245
275
315
345
375
400
425
455
485
515
545
575
0
25
50
75
100
Relative abundance [%]
Bathyarchaeota
Euryarchaeota
Lokiarchaeota
Thaumarchaeota
Others

863 **Figure 5**

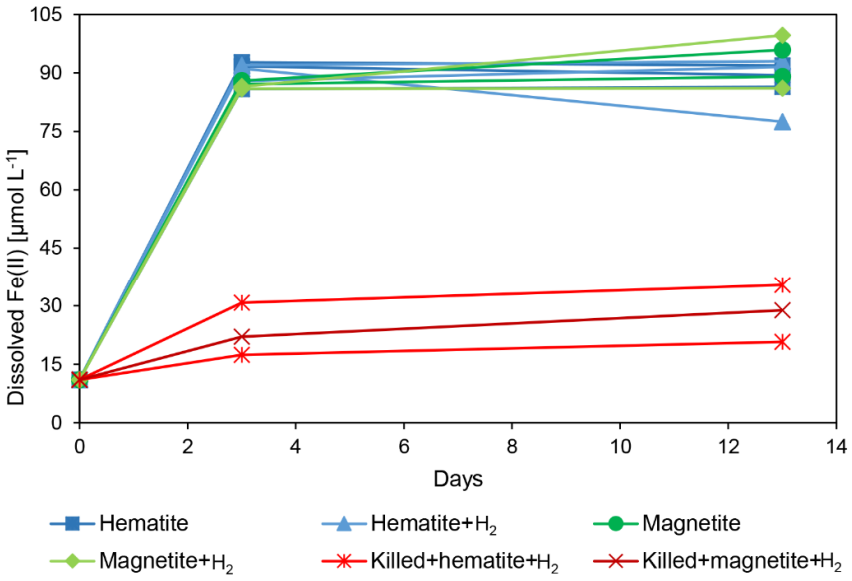

864

865

866 **Figure 6**

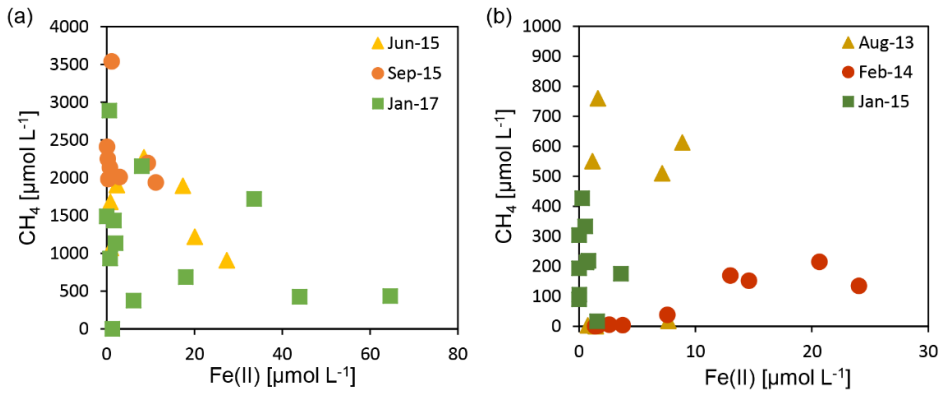

867

868

869

870

871

872

873

874